Cellulose (2021) 28:10305–10319
https://doi.org/10.1007/s10570-021-04202-0

ORIGINAL RESEARCH

Controllable Fe ion-anchored graphene heterostructures for robust and highly thermal conductive cellulose nanofiber composites

Bo Shan · Yuzhu Xiong

Received: 15 June 2021 / Accepted: 14 September 2021 / Published online: 24 September 2021

Abstract Developing the polymer-based thermal interface materials (TIMs) is one of the most promising approaches to address heat accumulation along with the functionalization, integration, and miniaturization of modern electronics, while it is still a great challenge to balance the thermal conductivity and mechanical properties. In this article, Fe ion-anchored graphene (FeG) is successfully fabricated by a facile in situ Fe reduction of graphene oxide (GO) approach, and then cellulose nanofibers (CNFs)/FeG composites are prepared by vacuum-assisted filtration. FeG exhibits excellent dispersion and exfoliation in CNFs/FeG composites, due to the strong interfacial interaction between CNFs and FeG, such as hydrogen bonds and "Fe–O" complex binding. Thus, CNFs/FeG composite has the largely improved thermal conductivity up to 30.2 W/mK at FeG content of 50 wt%, which is substantially increased by 1160% in comparison with that of pure CNFs. In addition, the mechanical performances of CNFs/FeG-50 are unexpectedly simultaneously enhanced to 244 MPa for tensile strength, 4.10% for elongation at break, and 9.5 GPa for Young's modulus, outperforming pure CNFs with increase of 137%, 33%, and 121%, respectively. This study provides a significant strategy for the design and construction of high thermal conductivity and high-performance polymeric TIMs in flexible and portable electronics.

B. Shan · Y. Xiong (✉)
Department of Polymer Materials and Engineering, College of Materials and Metallurgy, Guizhou University, Guiyang 550025, China
e-mail: xyzhu789@126.com

Present Address:
B. Shan
School of Materials Science and Engineering, Nankai University, National Institute for Advanced Materials, Tianjin 300000, China
e-mail: 1120190428@mail.nankai.edu.cn

Graphic Abstract

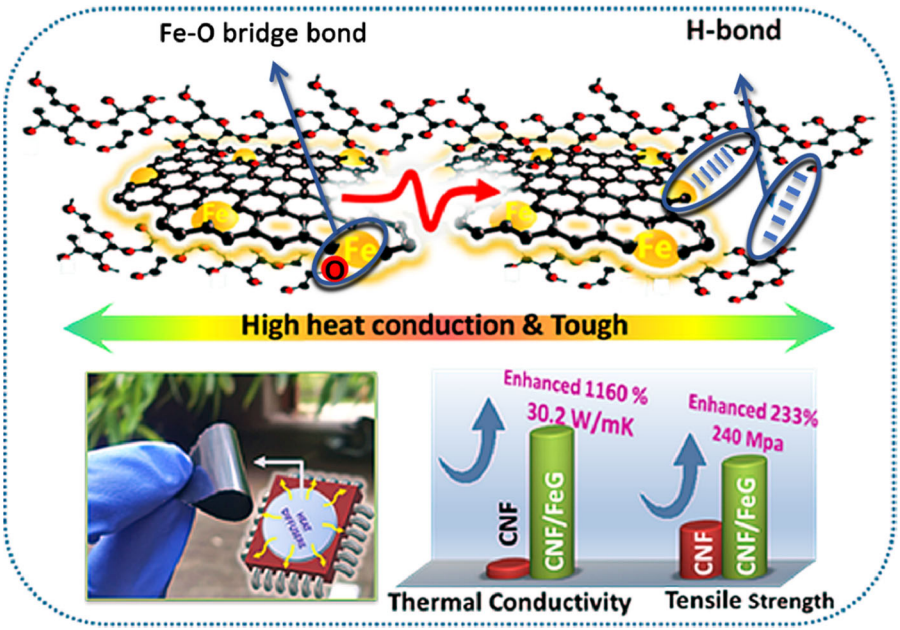

Keywords Cellulose nanofiber · Fe ion-anchored graphene · Thermal conductivity · Interfacial interaction · Mechanical properties

Introduction

Heat accumulation causes serious efficiency and safety issues in rapidly growing fields, such as aerospace, 5G communication, electric vehicles, and sophisticated equipment manufacturing (Song et al. 2018a, b; Ren et al. 2020; Chen et al. 2017). Central to this technical evolution is the development of composite materials having high thermal conductivity that can serve as thermal management materials (TMMs).

In order to realize the high-thermal conductivity ($K > 10$ W/mK) in composite materials, the design of 3D interconnection thermal conduction paths is regarded as a key factor to optimum utilization of filler. Han et al. (2019) reported a boron nitride (BNN)/epoxy composite based on nacre-mimetic 3D networks that exhibit the high thermal conductivity of 6.07 W/mK at 15 vol% BNN loading, together with outstanding electrical resistivity and thermal stability. Graphene, a superb thermally conducting filler, many researchers have been attracted to graphene because of its excellent thermal conductivity (5300 W/mK), high specific surface area and high aspect ratio (Song et al. 2018a,b; Balandin et al. 2008; Duan et al. 2020; Guo et al. 2021). Wu et al. revealed a significant synergistic effect between the aligned graphene nanosheets (GNs) and 3D interconnected graphene foam (GF), which plays a key role in the formation of thermal percolation networks, leading to the thermal conductivity of 11.16 W/mK at 10.27 vol% (Wu et al. 2019).

Apart from constructing artificial thermal conduction path through ice-templated self-assembly (Wu 2019; Schiffres 2013), liquid crystal induction (Meng et al. 2018; Ruan et al. 2021a, b; Ruan 2021), solvothermal synthesis (Xu 2010), melt migration limitation in block materials (Wu et al. 2017), etc., adding large amounts of well-dispersed fillers in the nanocomposites without excessive total mass or special processing methods is prone to multifunctional organic–inorganic hybrids (Xu et al. 2018a, 2018b). In most cases, the threshold is commonly about 30 vol.% to realize the connection heat conduction path in composites (Song et al. 2018a,b; Duan et al. 2020; Hu et al. 2017). Unfortunately, amounts of fillers may be detrimental to the mechanical performances and processibility, and lead to a large equivalent thermal resistance caused by agglomeration (Schiffres et al.

2013; Xu et al. 2018a,b; Yao et al. 2018; Guo et al. 2019; Ma et al. 2019).

Noticeably, previous studies have found that 1D cellulose nanofibers (CNFs) possess some abilities to disperse graphene in water solution and finally be combined together into a strong composite by hydrogen bonding (Jiang et al. 2018), thus eliminating the complex chemical modification process and increasing the process efficiency (Zhao et al. 2020; Zhuo 2018; Malho 2012; Hamedi 2014; Xu 2018). Malho et al. (2012) first mixed CNFs with multi-layer graphene, and then prepared a high-strength composite via intensely ultrasonic stripping (Malho 2012). The results demonstrated a simultaneous increase in Young's modulus (16.9 GPa), tensile strength (351 MPa), and toughness (22.3 MJ m^{-3}) for the obtained composite, due to the unique hydrogen bonding, dipole effect, hydrophobic–hydrophobic interaction, and CH–π interaction between CNFs and graphene (Hamedi 2014; Xu 2018; Chen 2018). However, with the increasing filler content, the mechanical properties can no longer keep up with high-strength applications, which is the common phenomenon in composites that lacks of specialized improvement (Malho 2012; Hamedi 2014; Xu 2018; Chen 2018; Shi 2021). For example, Yang et al. (2019) took advantage of the synergistic performance of the 2D expandable graphite nanoplatelet (EG), 1D CNFs, and flexible PEO. When the mass ratio of EG, CNFs, and PEO reached to 95:5:3, the graphene-based composite displayed a significantly increased thermal conductivity and a decreased tensile strength about 63.3 MPa. Cui et al. (2020) successfully prepared hybrids based on nanodiamonds (NDs), graphene sheets (GSs) and CNFs. The in-plane thermal conductivity of the hybrid at a filler content of 10 wt % could reach to 14.35 W/mK, and the moderate tensile strength was 90 Mpa. By contrast, balancing the thermal conductivity and mechanical properties under high loads is still a great challenge.

It is well known that the graphene oxides (GOs) contain the ability to disperse into high-concentration water solution, owing to the electrostatic repulsion generated by the ionization of oxygen-containing functional groups that are introduced by edge oxidation of the graphene (Yuan 2013; Tian 2016; Dong 2018). Moreover, heat transport in graphene has been taken considered to rely on electron and phonon, therefore, the in-plane integrity lattice is regarded as a key factor to reduce phonon scattering and has enhanced the thermal conductivity. We propose that a non-covalent modification method focused on edge binding of reduced GO (rGO) is a feasible strategy to balance the thermal conductivity and mechanical properties. Fan et al. (2011) reported that the sp^2 hybrid orbital lattice could be restored by the oxidation–reduction reaction with the participation of Fe ions, but the oxygen-containing functional group at the edge could be well remained. This controlled reduction of GO has achieved satisfactory results in terms of energy storage and adsorption separation. However, the role of edge-functionalized non-covalent modification graphene in thermal conductive composites has not been explored in detail yet.

In this paper, Fe ion-anchored graphene (FeG) is successfully in situ constructed via the controllable Fe-reduction of GO. FeG exhibits the high compatibility with CNFs, owing to the intense interaction between FeG and CNFs (e.g., hydrogen bonds and "Fe–O" complex bonds). Under vacuum filtration, CNFs/FeG composite possess the dense and compact structures with high in-plane alignment. As a consequence, the thermal conductivity of CNFs/FeG-50 is greatly enhanced, due to the continuous thermal conduction path built by aligned FeG sheets. The mechanical performances of CNFs/FeG-50 are also a lot higher than those of pure CNFs, due to the superb reinforcing effect of FeG. The flexible CNFs/FeG composites with both favorable thermal conductivity and mechanical properties open a potential application in microelectronics and advanced energy.

Material and methods

Materials

The cellulose nanofiber (CNF) dispersion with a carboxyl content of approximately 1.08 mol g^{-1} was provided by CANFOR Co., Ltd. (Canada). The mean diameter of CNFs is about 20 nm and the length is larger than 1 μm. All the parameters are kindly provided by the manufacturer. Graphene oxides (GOs) and graphene nano-plates (GNPs) were supplied by ENN Graphene Technology Co., Ltd (China). The anhydrous ethanol, Fe powder and HCl were purchased from Tianjin Kemio Chemical Reagent Co.,

Ltd (China). All the reagents were used without further purification.

Preparation of Fe ion-anchored graphene (FeG)

Figure 1 schematically shows the preparation method for FeG (Fan 2011). First, 10 g of graphene oxide weighed in a wide-mouth beaker and dispersed in 1 L of distilled water using a 600 W sonification. Secondly, 50 g of 300 mesh iron powder and 30 mL of 35 wt.% HCl solution were added into the above dispersion to allow the redox reaction. After 24 h reaction, the product was washed several times with deionized water to neutralization. Lastly, FeG was obtained by freeze-drying for 48 h.

Preparation of CNFs/FeG composites

For comparison, CNFs/GNP-50 was prepared by the same procedure. The homogeneous mixture suspensions with different FeG contents (0, 10, 30, and 50 wt.%) were prepared via mechanically stirring for 30 min and subsequent ultrasonic treatment for 20 min. Afterwards, the above suspensions were vacuum-filtered via a hydrophilic ester filter membrane with a pore size of 0.22 μm and diameter of 47 mm. The CNFs/FeG composites and pure CNFs were taken off from the substrate membranes after air-drying overnight at room temperature.

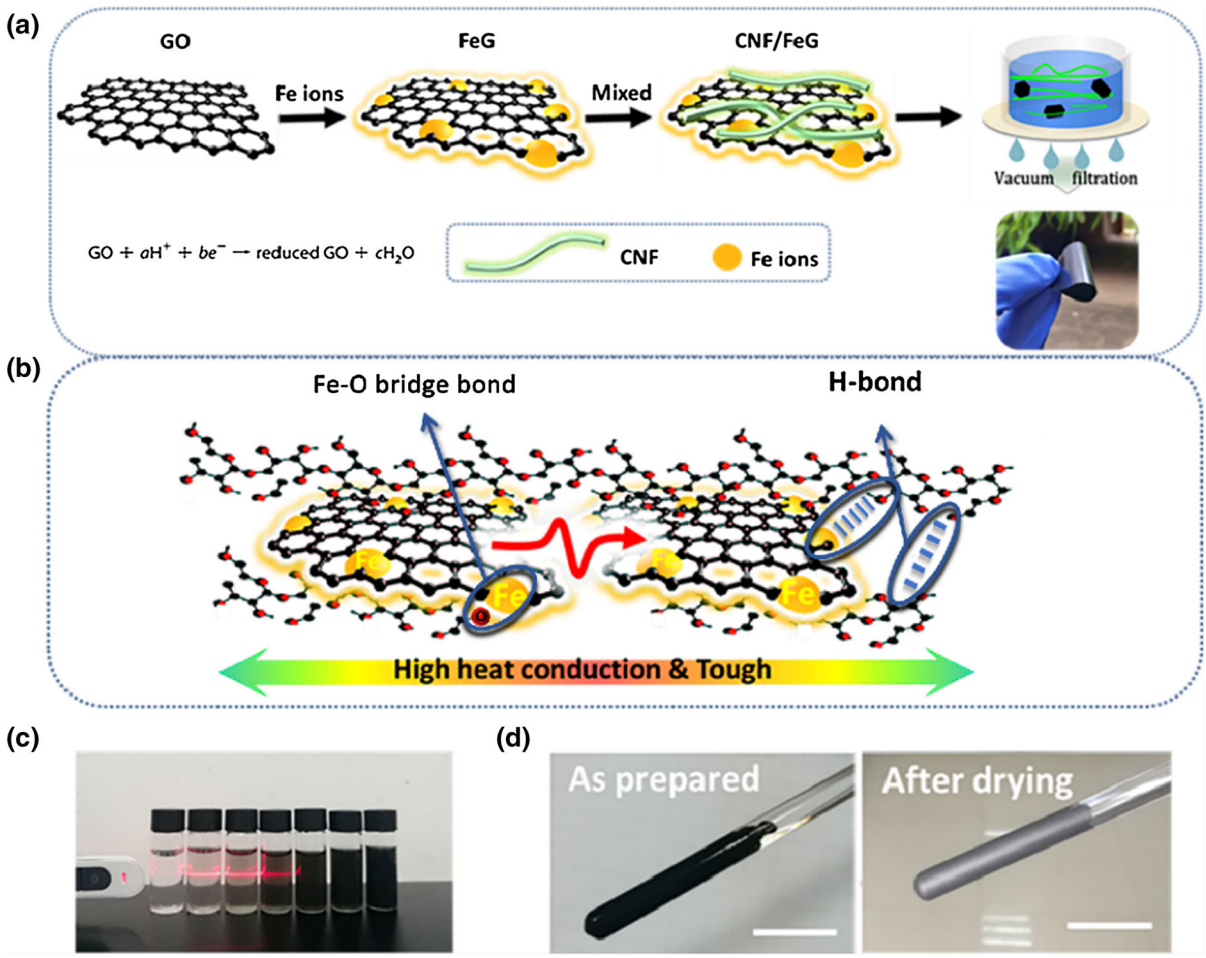

Fig. 1 **a** Schematic diagram of the preparation process of FeG and CNFs/FeG composites, **b** Schematic of the bridge binding between CNFs and FeG, **c** Optical photo of CNF/FeG aqueous suspensions, **d** Optical photos for FeG coating on a glass rod

Characterizations

Scanning electron microscope (SEM) images were obtained using a JSM-7500F microscope (JEOL, Japan) at an operating voltage of 5 kV. The X-ray diffraction (XRD) patterns were recorded on an X-ray diffractometer (D/max 2200, Rigaku, Japan) in Cu Kα radiation (k = 1.5406 Å) at 40 kV, scanning from 5° to 40° at a speed of 4°/min. After drying at 50 °C for 6 h, the chemical structures of hybrids were characterized through attenuated total reflectance Fourier-transform infrared (ATR-FTIR) spectroscopy (Nicolet iS50, U.S.A.) over the range of 4000–400 cm^{-1} and Raman spectroscopy (Renishaw Invia, U.K.) using a Ne-Ha laser. The "in-plane" mode thermal diffusion coefficient k was measured by the laser flash Netzsch LFA 467 at 25 °C. The thermal conductivity (K) was then determined as $K = \rho \cdot k \cdot C_P$, where ρ is the mass density measured by drainage method and C_P is the specific heat obtained by differential scanning calorimetry (DSC). The tensile properties of the obtained composites were measured using an Instron tester (INSTRON 5865) at a loading speed of 0.5 mm/min.

Discussion

Preparation and properties of FeG

The preparation process for FeG is intuitively illustrated in Fig. 1a. During the reduction of GO powder to FeG at the presence of Fe/Fe^{2+}, the volume is largely expanded, which greatly enhances the specific surface area of FeG and interfacial interaction between CNFs and FeG. The obtained FeG has a good dispersion in CNF aqueous solution, as shown in Fig. 1c. A dense and continuous FeG coating is formed on the glass rod (Fig. 1d), which proves that the obtained FeG also has good self-assembly activity nitride (Zhao 2017; Ramanathan 2008).

The Raman spectra of GO, FeG and GNP are comparatively shown in Fig. 2a. The peak intensity ratio I_D/I_G of FeG is remarkably decreased from 1.14 to 0.86 in contrast with that of GO, which indicates an improved in-plane π–π conjugated structure (Ferrari and Robertson 2000). Considering that the reduction process may lead to size reduction, the actual I_D/I_G value may be even lower (Ferrari 2000). D- and G-bands of FeG shift to lower wavenumber after reduction, mainly due to the Fe–O charge transfer (Geng 2013). This implies that parts of the oxygen-containing functional groups that preserved after the 24 h reduction mainly centered on the edge of graphene (Jha 2017). Moreover, the symmetrical second-order phonon scattering peak (i.e., 2D peak) of FeG located at 2700 cm^{-1} (532 nm) can be decomposed into four peaks, which indicates that a certain amount of bilayer graphene exists among FeG (Ni 2008). The XRD diagrams (Fig. 2b) show that the strong diffraction peak traced at 26° for GNP is corresponding to the plane lattice (002). However, the (002) plane diffraction peak of FeG is observed over a wide range of 21–26°, signifying a large amount of exfoliated graphene nanosheets (Cui 2011). Such a phenomenon takes place because Fe/Fe^{2+} ions are largely intercalated between GO layers as the reaction proceeds (Geng 2013). From the Bragg equation, the sharp shoulder peak at 21° in FeG XRD curve is corresponding to the planar spacing of about 4.2 Å, which indicates the existence of 1–2 layer graphene after the reduction. The SEM image of FeG is displayed in Fig. 2c. FeG exhibits a thin layer structure with many wrinkles, which indicates the pretty exfoliation of FeG (Stankovich 2006; Park 2014).

FTIR spectra are used to determine the types of oxygen-containing functional groups on FeG (Fig. 3). In GO, the broad and intense hydroxyl peak is situated at 3304 cm^{-1}, and the asymmetrical and symmetrical stretching vibrations of $–CH_2$ are located at 2925 and 2856 cm^{-1}, respectively. The prominent peak at about 1750 cm^{-1} is corresponding to ester C=O stretching vibration. The characteristic peaks indexed to carboxy/carbonyl and aromatic C=C stretching vibrations are observed at 1637 and 1539 cm^{-1}, respectively. The peak existing at 1222 cm^{-1} is assigned to epoxy C–O stretching vibration. The bands at 1150 and 1050 cm^{-1} are the respective stretching vibrations of the tertiary and primary alcohol C–O (Lu 2008).

After reduction by Fe/Fe^{2+}, the hydroxyl band centered at the higher wavenumber (3440 cm^{-1}) for FeG presents the observably decreased intensity, which illustrates the effective removal of oxygen-containing functional groups and the strong "Metal–Oxygen" (Fe–O) interaction (Scott 2013). Accordingly, the ester C=O (1750 cm^{-1}) and epoxy C–O (1222 cm^{-1}) bands are remarkably weakened with the

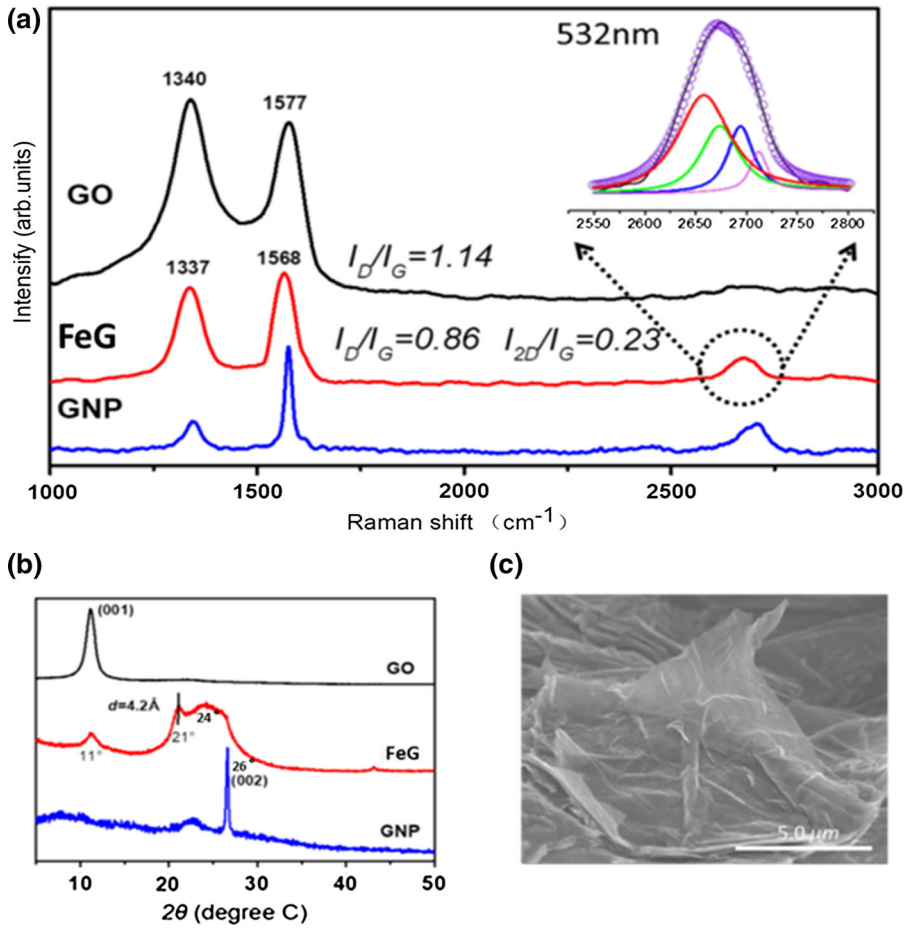

Fig. 2 **a** Raman spectra and (**b**) XRD patterns of GO, FeG and GNP, **c** SEM image of FeG

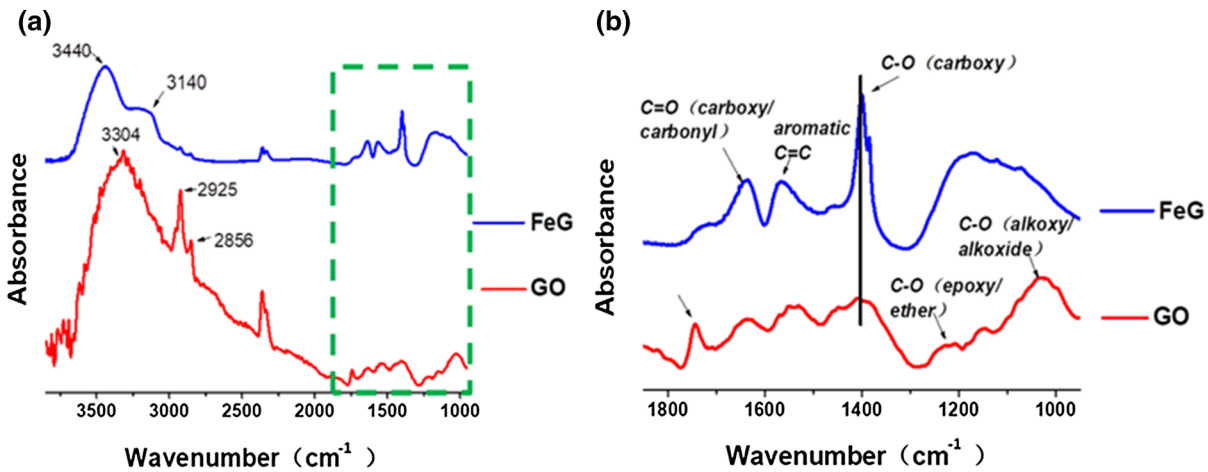

Fig. 3 FTIR spectra of FeG and GO in (**a**) 4000–1000 cm^{-1} and (**b**) 1800–1000 cm^{-1}

reduction proceeding, because of the reaction between the epoxy groups and Lewis alkali metal ions (He 1998; Lerf 1998). Natheless, the carboxy C=O and aromatic C=C are largely augmented, indicating the restored π-π conjugated structures. In addition, plenty of primary alcohol C–O bonds are converted to tertiary alcohol, possibly owing to the recovery of C–C bonds. The results infer that some certain oxygen-containing functional groups remain after Fe-reduction, most of which exist in the form of carboxyl groups at the edge of FeG sheets.

Morphology, structures and mechanical properties of CNFs/FeG composites

To explore the morphology and microstructures of CNFs/FeG composites, cross-section SEM images of CNFs/FeG-50 are depicted in Fig. 4a and b. At such high FeG loading of 50 wt%, CNFs/FeG-50 displays a highly aligned and ordered layer-by-layer structure, which is essential to the high performance of CNFs/FeG composites. This aligned structure heavily depends on the good dispersion and exfoliation of FeG at the assistance of CNFs/Fe ion. CNFs with large number of hydrophilic groups (–COOH and –OH) can be easily intercalated into FeG interlamination through the induction of Fe ions, which is profitable for the pretty dispersion and stability of FeG in CNF solution (Fig. 4d). As showed in Fig. 4c, the positive Fe ions introduced on FeG also play a pivotal role in assisting FeG exfoliation via the dynamic "Metal-O" bond interaction between Fe ions and CNFs in terms of CH-π interaction, dipole interaction, hydrophobic-hydrophobic interaction, etc. The interaction forces can act as the gripper of CNFs and FeG to strip more effectively FeG sheets under shear flow.

Figure 4e and f describe the FTIR spectra of pure CNFs and CNFs/FeG composites. It is visually found that the characteristic -OH peak slightly blue-shifts from 3252 cm^{-1} for pure CNFs to 3322 cm^{-1} for CNFs/FeG-50 with the increasing FeG content (Fig. 4f), which illustrates the strong hydrogen binding between FeG and CNFs. Similarly, C=O and C–O groups in carboxy moderately red-shifts with the addition of FeG content, due to a strong "Metal–Oxygen" complex bond between FeG and CNFs (Fig. 4e) (Zhao 2017; Kemp 2017). In brief, the interfacial interaction between FeG and CNFs in CNFs/FeG composites is largely enhanced with the introduction of Fe ions, which is vital to the improvement of mechanical properties of CNFs/FeG composites.

After the controllable reduction, the in-plane carbon lattice integrity of FeG is largely improved, so the stress load substantially increases in comparison with that of GO. Moreover, the complexation of Fe ions with oxygen-containing groups exerts a significant effect on the mechanical properties of CNFs/FeG composites. Figure 5a–c show the tensile properties of pure CNFs and CNFs/FeG composites. It is obviously observed that pure CNFs possesses the relatively poor mechanical poor mechanical performances, regrading strength of 103 MPa, elongation at break of 3.08%, and Young's modulus of 4.3 GPa. All the characteristic mechanical properties of CNFs/FeG composites are enhanced with the incremental FeG loadings. At a high FeG content of 50 wt%, the exceptionally improved strength, elongation at break, and Young's modulus reach up to 244 MPa, 4.10%, and 9.5 GPa, respectively, which is substantially increased by 137%, 33%, and 121%, respectively, in contrary to those of pure CNFs. This phenomenon is primely attributed to the strong interactions at CNFs/FeG interfaces concerning hydrogen bond and "Metal–Oxygen" bridge binding, which has been confirmed by the analyses of Raman and FTIR spectra. Generally speaking, a handful of metal ions can be penetrated into or through the interior space of graphene layers, limited by the radius of metal ions, which results in the insufficient interfacial bridge binding (Zhang 2018; Park 2008; Gong 2017; Wan 2018; Shen and Feng 2018). However, abundant Fe ions are anchored on FeG sheets by "Fe–O" complexation bonds during the controllable Fe reduction. The EDS line scanning spectrum (Fig. 5d) unveils the high Fe element fraction of 28.4 wt% in CNFs/FeG-50 composite. It is found in EDS mappings (Fig. 5e, f) that most Fe element is gathered at the FeG region, which manifests that Fe ions are firmly bonded on FeG sheet and not washed out in aqueous solution. The strongly anchored Fe ions on FeG can tightly link to CNFs via "Metal–Oxygen" bonds, contributing to the reinforced mechanical properties of CNFs/FeG composites.

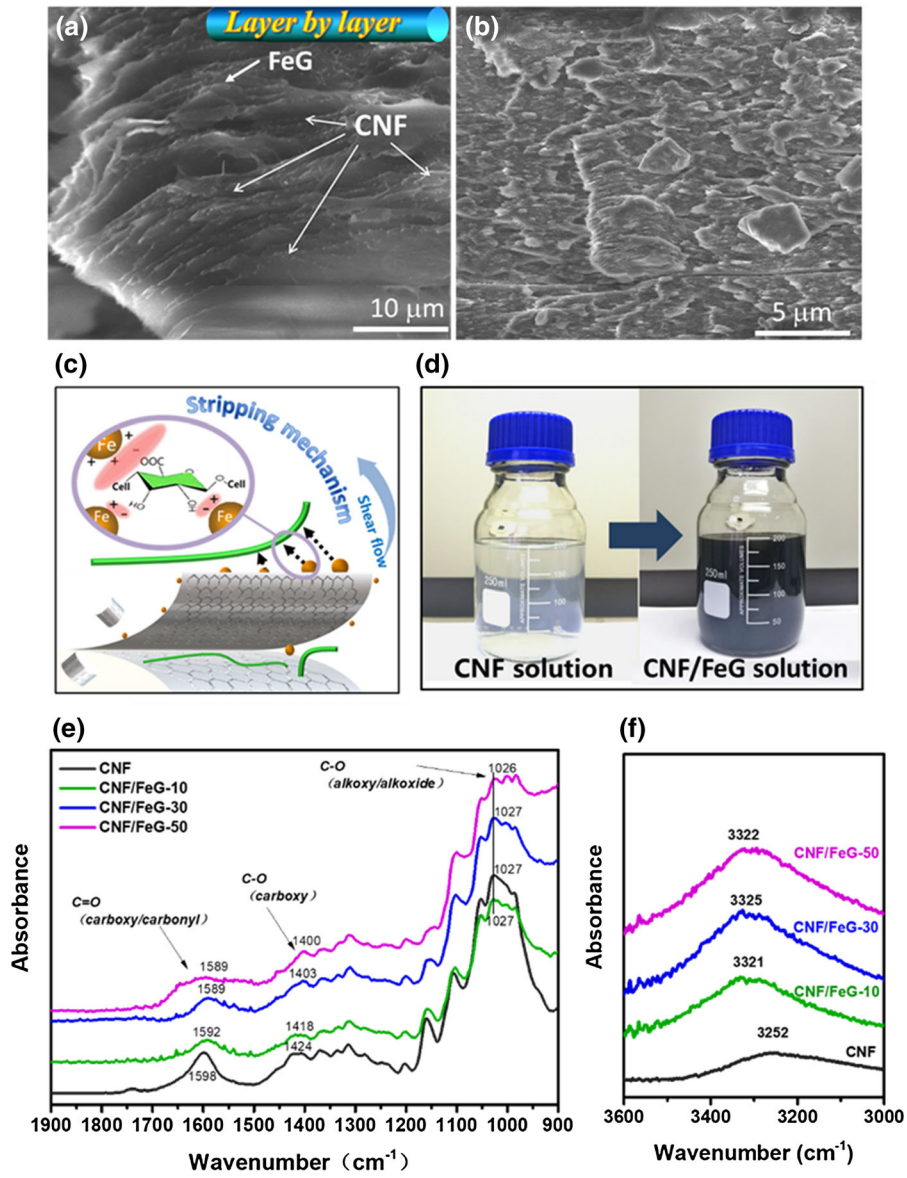

Fig. 4 **a**, **b** Cross-section SEM characterizations of CNFs/FeG-50 composite, **c** Schematic diagram of CNFs/FeG stripping and dispersion mechanism, **d** Digital pictures of CNFs and CNF/FeG aqueous dispersions, FTIR spectra of pure CNFs and CNFs/FeG composites in the wavenumber of (**e**) 1900–900 cm^{-1} and 3600–3000 cm^{-1} (**f**)

Analysis of thermal conductivity of CNFs/FeG composites

The in-plane thermal diffusivity and thermal conductivity of CNFs/FeG are shown in Fig. 6a and c. It is visual that the in-plane thermal conductivity of pure CNFs is merely 2.4 W/mK, in good agreement with previous reports (Shen 2018; Uetani 2016). The thermal conductivity of CNFs/FeG is evidently enhanced with the introduction of FeG. When 10 wt% FeG is added, the thermal conductivity of CNFs/FeG composite reaches up to 9.3 W/mK. However, the thermal conductivity of CNFs/FeG-30 is slight changed (9.7 W/mK), compared with that of CNFs/FeG-10. With the further increasing FeG content to 50 wt%, the thermal conductivity is sharply enhanced to 30.2 W/mK, showing the enhancement of 1160% in comparison with that of pure CNFs, due to the complete thermal conductive paths built by the connection of FeG sheets. Considering the tiny alteration in ρ and C_P of CNFs/FeG composites, the changing trend of thermal diffusivity k is related to thermal conductivity K. On the basis of the LFA-467 instrument, thermal diffusivity is expressed as:

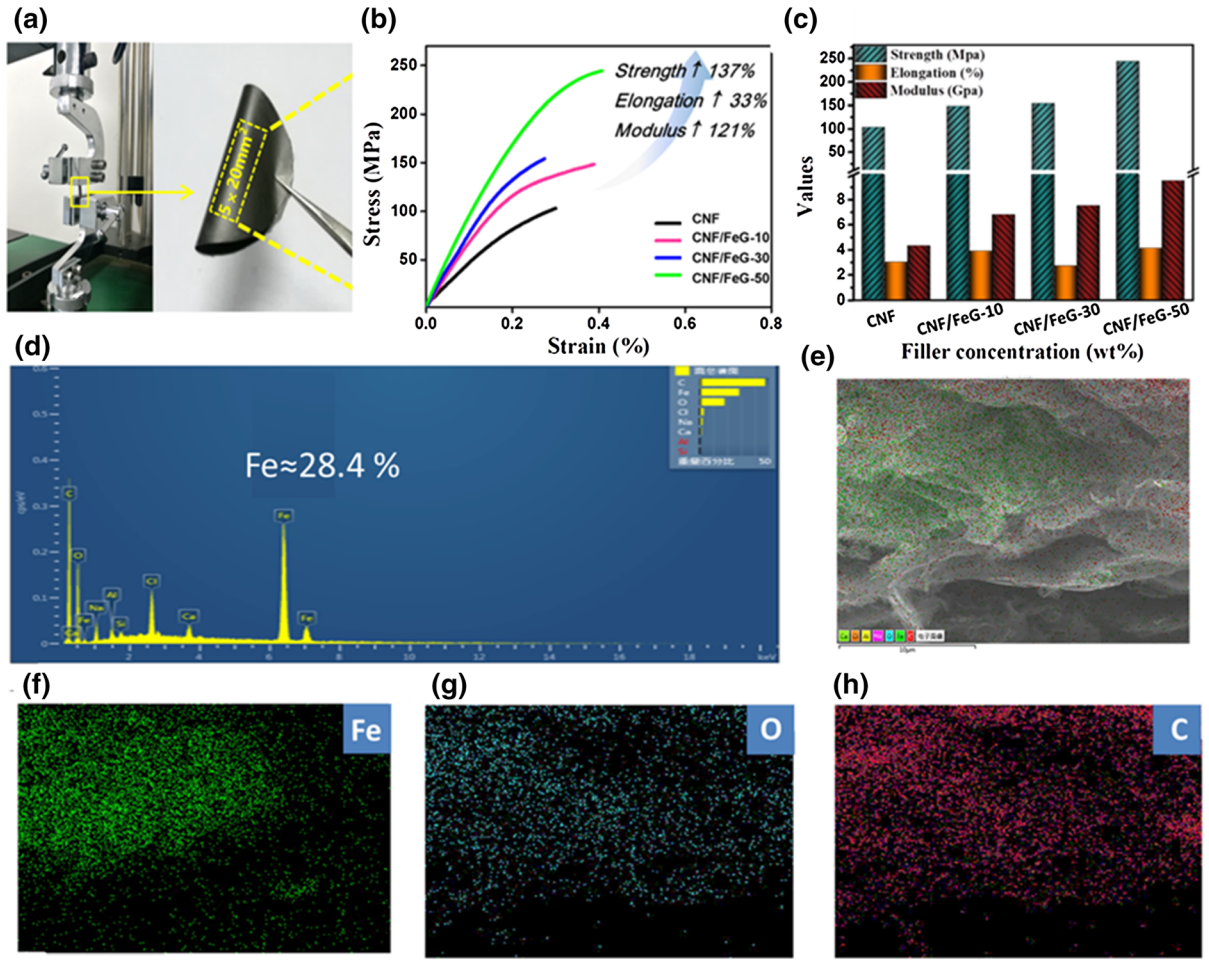

Fig. 5 **a** photos of mechanical tensile tester and CNFs/FeG composite, **b** Typical stress-train curves of pure CNFs and CNFs/FeG composites, **c** The corresponding strength, elongation, and modulus, **d** the EDS line scanning spectrum of CNFs/FeG-50, **e–h** EDS mapping images of CNFs/FeG-50

$$k = 0.1388 \cdot {L^2}/{t_{1/2}} \quad (1)$$

where $t_{1/2}$ is half of the time that it takes for the temperature to rise to the platform area and L is the sample thickness. We gather essential experimental evidences (Fig. 6b and d) and find that CNFs/FeG-50 expands the shortest $t_{1/2}$ (231 ms) to reach the temperature platform area, suggesting the highest thermal diffusivity (29.4 mm^2/s) and thermal conductivity (30.2 W/mK).

The heat conduction of graphene composites is enormously dependent on several key factors: (1) good exfoliation and dispersion of GO, (2) excellent oriented lamellae structures, and (3) satisfactory interface interaction (which can enhance the phonon resonance coupling). A great deal of in-plane aligned FeG with excellent exfoliation and dispersion has been identified in the developed composites. In addition, intense interface interaction between FeG and CNFs including hydrogen bond and "Fe–O" complex bridge binding is conductive to the construction of thermal conductive highway. A deductive mechanism related to the stack area of fillers is proposed in Fig. 7. The thermal conductivities of polymer composites are highly determined by the thermal conductivity of matrix, thermal conductivity of fillers, thermal resistance at matrix-filler interface, and thermal resistance at filler-filler interface (Gu 2021). Pure CNFs have a good thermal conductivity of 2.4 W/mK, which is greater than that of most polymer matrix, due to the

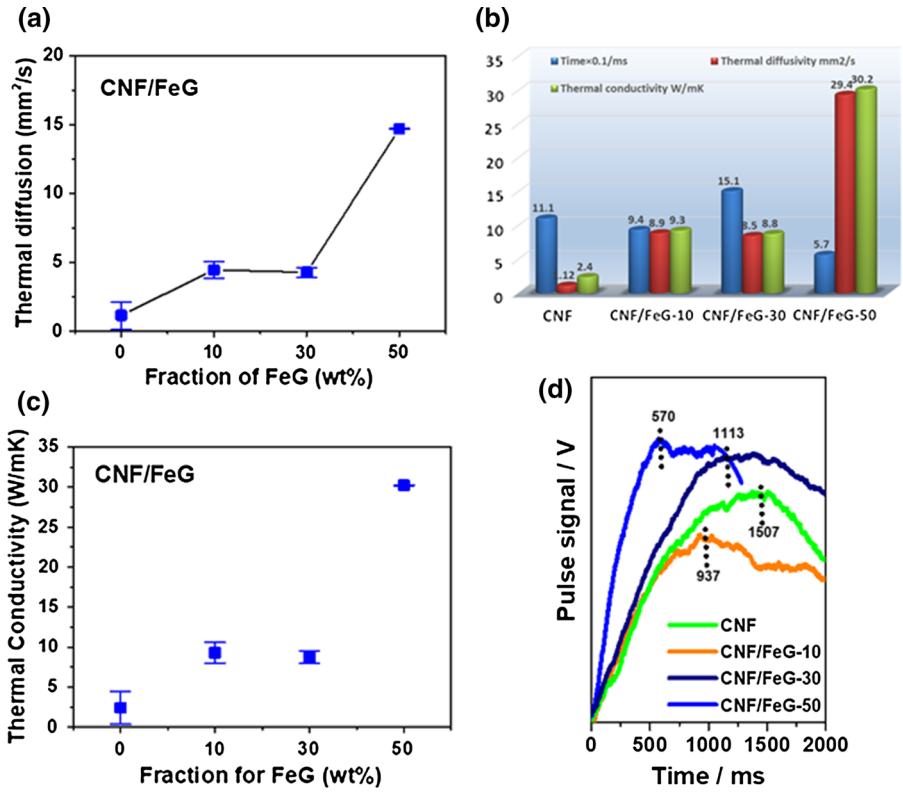

Fig. 6 **a** Thermal diffusivity and (**c**) thermal conductivity of CNFs/FeG composites with different FeG contents, **b** The relative comparison of pulse laser response time, thermal diffusivity, and thermal conductivity for CNFs/FeG composites, **d** The normalized Pulse signal-Time patterns for CNFs/FeG composites with different contents

wonderful aligned structures formed during the vacuum filtration. When the filler loading is less than 10 wt%, the thermal conductivity of CNFs/FeG composite is mainly leaned on the thermal conductivity and loading fraction of fillers. With the increasing FeG loading, the phonon scattering in insulating matrix has a large decrease, contributing to the improved thermal conductivity. Although the insulating bulk is reduced with the increasing FeG content at the filler range of 10–30 wt%, a large amount of FeG breaks the in-plane orientation structures of CNFs. Thus, the thermal conductivities of CNFs/FeG composites are slightly changed with the increasing FeG content in this region. At the FeG content higher than 30 wt%, FeG sheets begin to contact with each other and build the thermally conducting highway. In this stage, the thermal conductivity is primely dependent on the filler-filler thermal interfacial resistance and sharply enhanced up to 30.2 W/mK.

To emphasize the advantages of CNFs/FeG composites in thermal conduction and mechanical properties, we compared the developed composites with common CNFs/GNP composites, which is given in Fig. 8. As above mentioned, high filler loading will cause insufficient interfacial bonding, agglomeration of fillers, and formation of air pockets, which makes the composites brittle and difficult to process. Although CNFs can disperse and strip multilayer graphene to some extent (Malho 2012; Hamedi 2014; Xu 2018; Chen 2018), its effectiveness is strongly dependent on the mixing operation technology. In control experiments, CNFs/GNP-50 is too brittle to fabricate the complete circle film, despite having the similar thermal conduction level (Fig. 8a and b). SEM

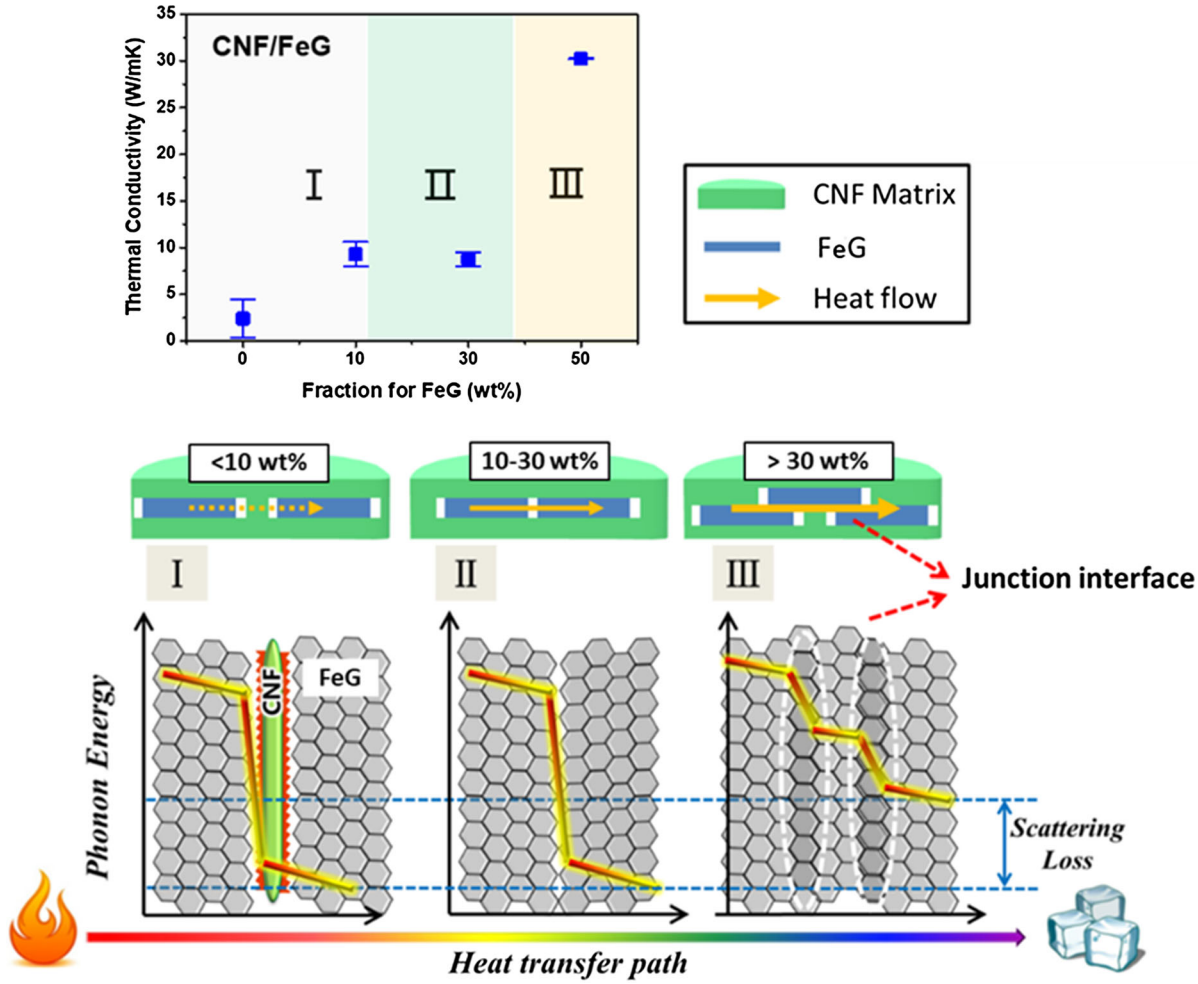

Fig. 7 Schematic diagram for the thermal conduction mechanism of CNFs/FeG

observations are conducted to in depth investigate the difference of microstructures between CNFs/FeG-50 and CNFs/GNP-50 (Fig. 8c–f). The images reveal that CNFs/FeG-50 is a dense and robust composite with pretty in-plane orientation structures. Nonetheless, CNFs/GNO displays a coarse, loose, and disordered microstructure, giving rise to the inferior strength that cannot support tensile tests.

In order to estimate the contribution of this present investigation, the comparison of thermal conduction and mechanical properties in CNFs/FeG composites with the reported values in other polymeric composites have summarized in Fig. 9. Visibly, it is quite difficult to achieve simultaneously superior thermal conductivity and mechanical properties in the case of polymer-based composites. In this effort, CNFs/FeG composites display high-level thermal conductivity and mechanical properties at the same time, which surpasses the most reported composites in previous literatures. The comparison results clearly illuminate

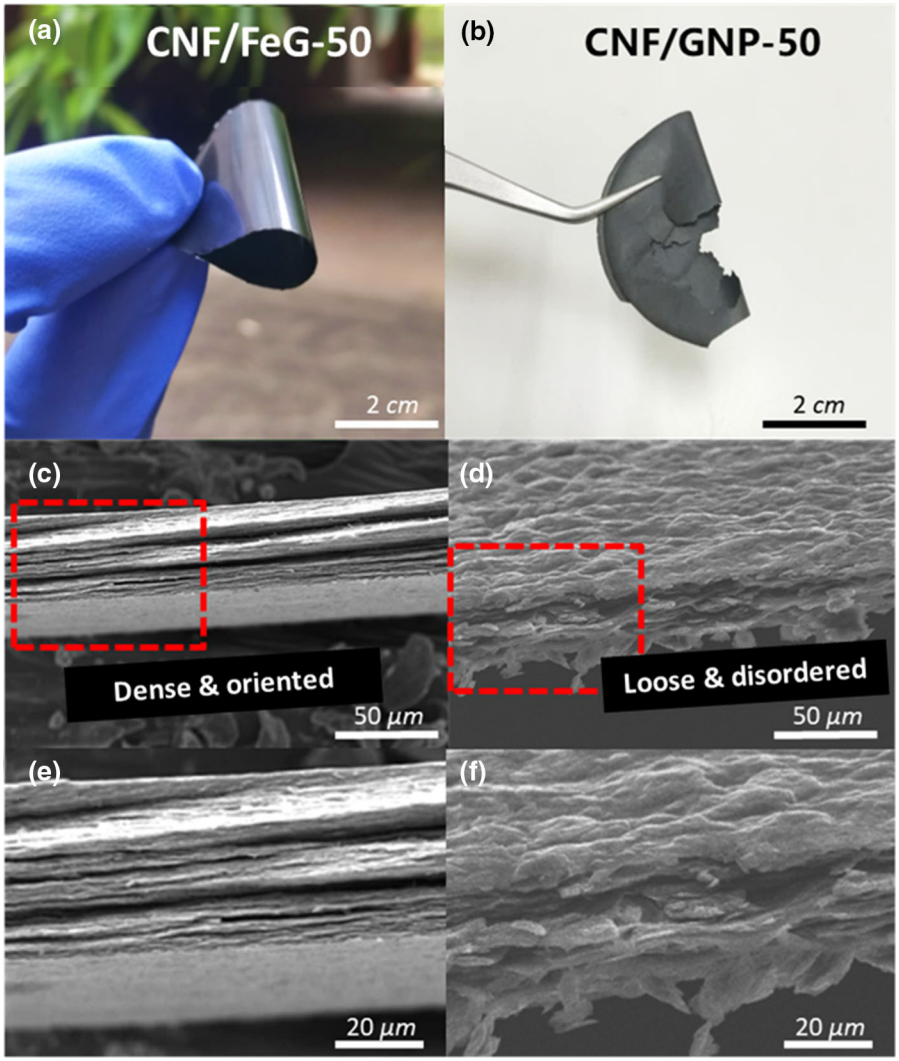

Fig. 8 **a**, **b** Comparison of optical photos of CNFs/FeG-50 and CNFs/GNP-50 composites, **c**, **d** Cross-sectional SEM images of CNFs/FeG-50 and CNFs/GNP-50, respectively, **e**, **f** Partial enlarged SEM images in (**c** and **d**)

that the proposed method is competitive to promote dramatically mechanical properties and thermal conductivities of CNF composites.

Conclusion

In conclusion, a creative interfacial control strategy is proposed to fabricate polymeric composites with both fascinating thermal conductivity and mechanical performance. Fe ion-anchored graphene (FeG) are produced via in situ reduction of GO with Fe/Fe^{2+}, followed by being incorporated into CNFs matrix by a vacuum filtration method. The Raman and FTIR spectra clearly reveal that FeG has been reduced effectively, and Fe ions are tightly anchored on FeG sheets via strong "Fe–O" complex bonds. FeG shows the wonderful exfoliation and dispersion with the help of CNFs in aqueous solution, which attributed to the intense interaction between FeG and CNFs. Moreover, CNFs/FeG composites have pretty in-plane orientation structures under the vacuum filtration. At FeG content of 50 wt%, the thermal conductivity is sharply enhanced to 30.2 W/mK, showing the enhancement of 1160% in comparison with that of pure CNFs, due to the complete thermal conductive paths built by the

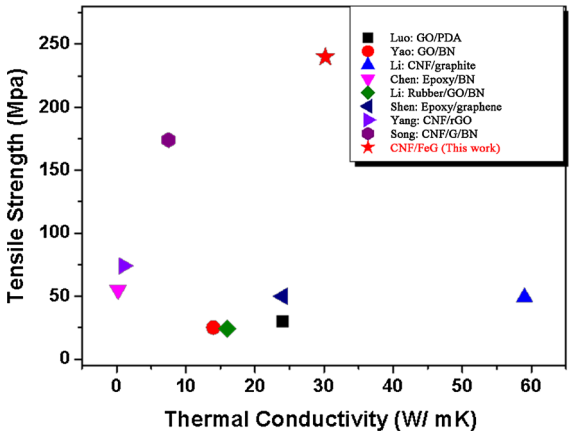

Fig. 9 Comparison of thermal conductivity and tensile strength for different polymer-based composites (Luo 2017; Yao 2016; Li 2017; Chen 2020; Li 2020; Shen 2016; Yang 2017; Song 2018)

connection of FeG sheets. In addition, CNFs/FeG-50 exhibits the exceptionally simultaneous increment of tensile strength (137%), elongation at break (33%), and Young's modulus (121%), in contrast with pure CNFs. Hence, this strategy provides a valuable insight into the design and construction of high-thermal-conductivity and high-performance polymer composites for versatile application in modern electronic devices.

Acknowledgments This work was supported by the National Natural Science Foundation of China (NSFC No. 51663003); Science and Technology Foundation of Guizhou Province (Grant No. [2019] 2166).

Declarations

Conflict of interest We have no conflicts of interest to declare that are relevant to the content of this article. We certify that they have no affiliations with or involvement in any organization or entity with any financial interest or non-financial interest in the subject matter or materials discussed in this manuscript. We have no financial or proprietary interests in any material discussed in this article.

Human and animal rights This article does not contain any studies with human participants or animals performed by any of the authors. All the experiments were undertaken in this study comply with the current laws of the country where they were performed.

Data availability All data generated or analyzed during this study are included in this published article.

References

Balandin AA, Ghosh S, Bao W, Calizo I, Teweldebrhan D, Miao F, Lau CN (2008) Superior thermal conductivity of single-layer graphene. Nano Lett 8:902–907. https://doi.org/10.1021/nl0731872

Chen G, Chen T, Hou K, Ma W, Tebyetekerwa M, Cheng Y, Weng W, Zhu M (2018) Robust, hydrophilic graphene/cellulose nanocrystal fiber-based electrode with high capacitive performance and conductivity. Carbon 127:218–227. https://doi.org/10.1016/j.carbon.2017.11.012

Chen J, Huang X, Zhu Y, Jiang P (2017) Cellulose nanofiber supported 3D interconnected BN nanosheets for epoxy nanocomposites with ultrahigh thermal management capability. Adv Funct Mater 27:1604754. https://doi.org/10.1002/adfm.201604754

Chen X, Lim JSK, Yan W, Guo F, Liang YN, Chen H, Lambourne A, Hu X (2020) Salt template assisted BN scaffold fabrication toward highly thermally conductive epoxy composites. ACS Appl Mater Interfaces 12:16987–16996. https://doi.org/10.1021/acsami.0c04882

Cui P, Lee J, Hwang E, Lee H (2011) One-pot reduction of graphene oxide at subzero temperatures. Chem Commun 47:12370–12372. https://doi.org/10.1039/C1CC15569E

Cui S, Song N, Shi L, Ding P (2020) Enhanced thermal conductivity of bioinspired nanofibrillated cellulose hybrid films based on graphene sheets and nanodiamonds. ACS Sustain Chem Eng 8:6363–6370. https://doi.org/10.1021/acssuschemeng.0c00420

Dong L, Chen Z, Zhao X, Ma J, Lin S, Li M, Bao Y, Chu L, Leng K, Lu H (2018) A non-dispersion strategy for large-scale production of ultra-high concentration graphene slurries in water. Nat Commun 9:1–8. https://doi.org/10.1038/s41467-017-02580-3

Duan H, Zhu H, Gao J, Yan D, Dai K, Yang Y, Zhao G, Liu Y, Li Z (2020) Asymmetric conductive polymer composite foam for absorption dominated ultra-efficient electromagnetic interference shielding with extremely low reflection characteristics. J Mater Chem A 8:9146–9159. https://doi.org/10.1039/D0TA01393E

Fan ZJ, Kai W, Yan J, Wei T, Zhi LJ, Feng J, Ren YM, Song LP, Wei F (2011) Facile synthesis of graphene nanosheets via Fe reduction of exfoliated graphite oxide. ACS Nano 5:191–198. https://doi.org/10.1021/nn102339t

Ferrari AC, Robertson J (2000) Interpretation of Raman spectra of disordered and amorphous carbon. Phys Rev B 61:14095. https://doi.org/10.1103/PhysRevB.61.14095

Geng X, Guo Y, Li D, Li W, Zhu C, Wei X, Chen M, Gao S, Qiu S, Gong Y (2013) Interlayer catalytic exfoliation realizing scalable production of large-size pristine few-layer graphene. Sci Rep 3:1–6. https://doi.org/10.1038/srep01134

Gong S, Zhang Q, Wang R, Jiang L, Cheng Q (2017) Synergistically toughening nacre-like graphene nanocomposites via gel-film transformation. J Mater Chem A 5:16386–16392. https://doi.org/10.1039/C7TA03535G

Guo Y, Yang X, Ruan K, Kong J, Dong M, Zhang J, Gu J, Guo Z (2019) Reduced graphene oxide heterostructured silver nanoparticles significantly enhanced thermal conductivities in hot-pressed electrospun polyimide nanocomposites.

ACS Appl Mater Interfaces 11:25465–25473. https://doi.org/10.1021/acsami.9b10161

Guo Y, Ruan K, Gu J (2021) Controllable thermal conductivity in composites by constructing thermal conduction networks. Mater Today Phys 20:100449. https://doi.org/10.1016/j.mtphys.2021.100449

Gu J, Ruan K (2021) Breaking through bottlenecks for thermally conductive polymer composites: a perspective for intrinsic thermal conductivity, interfacial thermal resistance and theoretics. Nano-Micro Lett 13:1–9. https://doi.org/10.1007/s40820-021-00640-4

Hamedi MM, Hajian A, Fall AB, Håkansson K, Salajkova M, Lundell F, Wågberg L, Berglund LA (2014) Highly conducting, strong nanocomposites based on nanocellulose-assisted aqueous dispersions of single-wall carbon nanotubes. ACS Nano 8:2467–2476. https://doi.org/10.1021/nn4060368

Han J, Du G, Gao W, Bai H (2019) An anisotropically high thermal conductive boron nitride/epoxy composite based on nacre-mimetic 3D network. Adv Funct Mater 29:1900412. https://doi.org/10.1002/adfm.201900412

He H, Klinowski J, Forster M, Lerf A (1998) A new structural model for graphite oxide. Chem Phys Lett 287:53–56. https://doi.org/10.1016/S0009-2614(98)00144-4

Hu J, Huang Y, Yao Y, Pan G, Sun J, Zeng X, Sun R, Xu JB, Song B, Wong CP (2017) Polymer composite with improved thermal conductivity by constructing a hierarchically ordered three-dimensional interconnected network of BN. ACS Appl Mater Interfaces 9:13544–13553. https://doi.org/10.1021/acsami.7b02410

Jha PK, Singh SK, Kumar V, Rana S, Kurungot S, Ballav N (2017) High-level supercapacitive performance of chemically reduced graphene oxide. Chem 3:846–860. https://doi.org/10.1016/j.chempr.2017.08.011

Jiang F, Li T, Li Y, Zhang Y, Gong A, Dai J, Hitz E, Luo W, Hu L (2018) Wood-based nanotechnologies toward sustainability. Adv Mater 30:1703453. https://doi.org/10.1002/adma.201703453

Kemp W (2017) Organic spectroscopy. Macmillan International Higher Education, London

Lerf A, He H, Forster M, Klinowski J (1998) Structure of graphite oxide revisited. J Phys Chem B 102:4477–4482. https://doi.org/10.1021/jp9731821

Li G, Tian X, Xu X, Zhou C, Wu J, Li Q, Zhang L, Yang F, Li Y (2017) Fabrication of robust and highly thermally conductive nanofibrillated cellulose/graphite nanoplatelets composite papers. Compos Sci Technol 138:179–185. https://doi.org/10.1016/j.compscitech.2016.12.001

Li J, Zhao X, Wu W, Zhang Z, Xian Y, Lin Y, Lu Y, Zhang L (2020) Advanced flexible rGO-BN natural rubber films with high thermal conductivity for improved thermal management capability. Carbon 162:46–55. https://doi.org/10.1016/j.carbon.2020.02.012

Lu J, Askeland P, Drzal LT (2008) Surface modification of microfibrillated cellulose for epoxy composite applications. Polymer 49:1285–1296. https://doi.org/10.1016/j.polymer.2008.01.028

Luo L, Wu K, Shi J, Du X, Li X, Yang L, Lu M (2017) Green reduction of graphene oxide by polydopamine to a construct flexible film: superior flame retardancy and high thermal conductivity. J Mater Chem A 5:18542–18550. https://doi.org/10.1039/C7TA04740A

Ma T, Zhao Y, Ruan K, Liu X, Zhang J, Guo Y, Yang X, Kong J, Gu J (2019) Highly thermal conductivities, excellent mechanical robustness and flexibility, and outstanding thermal stabilities of aramid nanofiber composite papers with nacre-mimetic layered structures. ACS Appl Mater Interfaces 12:1677–1686. https://doi.org/10.1021/acsami.9b19844

Malho JM, Laaksonen PI, Walther A, Ikkala O, Linder MB (2012) Facile method for stiff, tough, and strong nanocomposites by direct exfoliation of multilayered graphene into native nanocellulose matrix. Biomacromol 13:1093. https://doi.org/10.1021/bm2018189

Meng X, Pan H, Zhu C, Chen Z, Lu T, Xu D, Li Y, Zhu S (2018) Coupled chiral structure in graphene-based film for ultrahigh thermal conductivity in both in-plane and through-plane directions. ACS Appl Mater Interfaces 10:22611–22622. https://doi.org/10.1021/acsami.8b05514

Ni Z, Wang Y, Yu T, Shen Z (2008) Raman spectroscopy and imaging of graphene. Nano Res 1:273–291. https://doi.org/10.1007/s12274-008-8036-1

Park S, Lee KS, Bozoklu G, Cai W, Nguyen ST, Ruoff RS (2008) Graphene oxide papers modified by divalent ions—enhancing mechanical properties via chemical cross-linking. ACS Nano 2:572–578. https://doi.org/10.1021/nn700349a

Park W, Hu J, Jauregui LA, Ruan X, Chen YP (2014) Electrical and thermal conductivities of reduced graphene oxide/polystyrene composites. Appl Phys Lett 104:113101. https://doi.org/10.1063/1.4869026

Ramanathan T, Abdala A, Stankovich S, Dikin D, Herrera-Alonso M, Piner R, Adamson D, Schniepp H, Chen X, Ruoff R (2008) Functionalized graphene sheets for polymer nanocomposites. Nat Nanotechnol 3:327–331. https://doi.org/10.1038/nnano.2008.96

Ren W, Zhu H, Yang Y, Chen Y, Duan H, Zhao G, Liu Y (2020) Flexible and robust silver coated non-woven fabric reinforced waterborne polyurethane films for ultra-efficient electromagnetic shielding. Compos Part B-Eng 184:107745. https://doi.org/10.1016/j.compositesb.2020.107745

Ruan K, Guo Y, Gu J (2021a) Liquid crystalline polyimide films with high intrinsic thermal conductivities and robust toughness. Macromolecules 54:4934–4944. https://doi.org/10.1021/acs.macromol.1c00686

Ruan K, Zhong X, Shi X, Dang J, Gu J (2021b) Liquid crystal epoxy resins with high intrinsic thermal conductivities and their composites: a mini-review. Mater Today Phys 20:100456. https://doi.org/10.1016/j.mtphys.2021.100456

Schiffres SN, Harish S, Maruyama S, Shiomi J, Malen JA (2013) Tunable electrical and thermal transport in ice-templated multilayer graphene nanocomposites through freezing rate control. ACS Nano 7:11183–11189. https://doi.org/10.1021/nn404935m

Scott AI (2013) Interpretation of the ultraviolet spectra of natural products: international series of monographs on organic chemistry. Elsevier, Amsterdams, p 7

Shen X, Wang Z, Wu Y, Liu X, He YB, Kim JK (2016) Multilayer graphene enables higher efficiency in improving thermal conductivities of graphene/epoxy composites.

Nano Lett 16:3585–3593. https://doi.org/10.1021/acs.nanolett.6b00722

Shen Z, Feng J (2018) Highly thermally conductive composite films based on nanofibrillated cellulose in situ coated with a small amount of silver nanoparticles. ACS Appl Mater Interfaces 10:24193–24200. https://doi.org/10.1021/acsami.8b07249

Shi X, Zhang R, Ruan K, Ma T, Guo Y, Gu J (2021) Improvement of thermal conductivities and simulation model for glass fabrics reinforced epoxy laminated composites via introducing hetero-structured BNN-30@ BNNS fillers. J Mater Sci Technol 82:239–249. https://doi.org/10.1016/j.jmst.2021.01.018

Song H, Liu J, Liu B, Wu J, Cheng HM, Kang F (2018a) Two-dimensional materials for thermal management applications. Joule 2:442–463. https://doi.org/10.1016/j.joule.2018.01.006

Song N, Pan H, Liang X, Cao D, Shi L, Ding P (2018b) Structural design of multilayer thermally conductive nanofibrillated cellulose hybrid film with electrically insulating and antistatic properties. J Mater Chem C 6:7085–7091. https://doi.org/10.1039/C8TC01277F

Stankovich S, Dikin DA, Dommett GH, Kohlhaas KM, Zimney EJ, Stach EA, Piner RD, Nguyen ST, Ruoff RS (2006) Graphene-based composite materials. Nature 442:282–286. https://doi.org/10.1038/nature04969

Tian S, Sun J, Yang S, He P, Wang G, Di Z, Ding G, Xie X, Jiang M (2016) Controllable edge oxidation and bubbling exfoliation enable the fabrication of high quality water dispersible graphene. Sci Rep 6:34127. https://doi.org/10.1038/srep34127

Uetani K, Okada T, Oyama HT (2016) Thermally conductive and optically transparent flexible films with surface-exposed nanocellulose skeletons. J Mater Chem C 4:9697–9703. https://doi.org/10.1039/C6TC03318K

Wan S, Fang S, Jiang L, Cheng Q, Baughman RH (2018) Strong, conductive, foldable graphene sheets by sequential ionic and π bridging. Adv Mater 30:1802733. https://doi.org/10.1002/adma.201802733

Wu D, Gao X, Sun J, Wu D, Liu Y, Kormakov S, Zheng X, Wu L, Huang Y, Guo Z (2017) Spatial confining forced network assembly for preparation of high-performance conductive polymeric composites. Compos Part A-Appl S 102:88–95. https://doi.org/10.1016/j.compositesa.2017.07.027

Wu Z, Xu C, Ma C, Liu Z, Cheng HM, Ren W (2019) Synergistic effect of aligned graphene nanosheets in graphene foam for high-performance thermally conductive composites. Adv Mater 31:1900199. https://doi.org/10.1002/adma.201900199

Xu X, Chen J, Zhou J, Li B (2018a) Thermal conductivity of polymers and their nanocomposites. Adv Mater 30:1705544. https://doi.org/10.1002/adma.201705544

Xu Y, Sheng K, Li C, Shi G (2010) Self-assembled graphene hydrogel via a one-step hydrothermal process. ACS Nano 4:4324–4330. https://doi.org/10.1021/nn101187z

Xu Y, Yang Y, Yan D, Duan H, Zhao G, Liu Y (2018b) Gradient structure design of flexible waterborne polyurethane conductive films for ultraefficient electrimagnetic shielding with low reflection characteristic. ACS Appl Mater Interfaces 10:19143–19152. https://doi.org/10.1021/acsami.8b05129

Yang W, Gong Y, Zhao X, Liu T, Zhang Y, Chen F, Fu Q (2019) Strong and highly conductive graphene composite film based on the nanocellulose-assisted dispersion of expanded graphite and incorporation of poly (ethylene oxide). ACS Sustain Chem Eng 7:5045–5056. https://doi.org/10.1021/acssuschemeng.8b05850

Yang W, Zhao Z, Wu K, Huang R, Liu T, Jiang H, Chen F, Fu Q (2017) Ultrathin flexible reduced graphene oxide/cellulose nanofiber composite films with strongly anisotropic thermal conductivity and efficient electromagnetic interference shielding. J Mater Chem C 5:3748–3756. https://doi.org/10.1039/C7TC00400A

Yao Y, Zeng X, Wang F, Sun R, Xu JB, Wong CP (2016) Significant enhancement of thermal conductivity in bioinspired freestanding boron nitride papers filled with graphene oxide. Chem Mater 28:1049–1057. https://doi.org/10.1021/acs.chemmater.5b04187

Yao Y, Zhu X, Zeng X, Sun R, Xu JB, Wong CP (2018) Vertically aligned and interconnected SiC nanowire networks leading to significantly enhanced thermal conductivity of polymer composites. ACS Appl Mater Interfaces 10:9669–9678. https://doi.org/10.1021/acsami.8b00328

Yuan W, Zhou Y, Li Y, Li C, Peng H, Zhang J, Liu Z, Dai L, Shi G (2013) The edge-and basal-plane-specific electrochemistry of a single-layer graphene sheet. Sci Rep 3:2248. https://doi.org/10.1038/srep02248

Zhang Y, Peng J, Li M, Saiz E, Wolf SE, Cheng Q (2018) Bioinspired supertough graphene fiber through sequential interfacial interactions. ACS Nano 12:8901–8908. https://doi.org/10.1021/acsnano.8b04322

Zhao L, Roh K, Kacmoli S, Kurdi KA, Jhulki S, Barlow S, Marder SR, Gmachl C, Rand BP (2020) Thermal management enables bright and stable perovskite light-emitting diodes. Adv Mater 32:2000752. https://doi.org/10.1002/adma.202000752

Zhao X, Gao W, Yao W, Jiang Y, Xu Z, Gao C (2017) Ion diffusion-directed assembly approach to ultrafast coating of graphene oxide thick multilayers. ACS Nano 11:9663–9670. https://doi.org/10.1021/acsnano.7b03480

Zhuo H, Zhang H, Wang L, Lu Q, Kaplan DL (2018) Sonication exfoliation of defect-free graphene in aqueous silk nanofiber solutions. ACS Sustain Chem Eng 6:12261–12267. https://doi.org/10.1021/acssuschemeng.8b02644